Hindawi Publishing Corporation
Journal of Nanomaterials
Volume 2015, Article ID 395483, 8 pages
http://dx.doi.org/10.1155/2015/395483

Research Article

Synthesis of Monodisperse Walnut-Like SnO_2 Spheres and Their Photocatalytic Performances

Jing Wang,[1,2] Hui-qing Fan,[1] and Hua-wa Yu[2]

[1]*State Key Laboratory of Solidification Processing, School of Materials Science and Engineering, Northwestern Polytechnical University, Xi'an 710072, China*
[2]*School of Science, Xi'an Polytechnic University, Xi'an 710048, China*

Correspondence should be addressed to Hui-qing Fan; hqfan3@163.com

Received 26 May 2015; Revised 27 August 2015; Accepted 7 September 2015

Academic Editor: Pantaleo D. Cozzoli

Novel walnut-like SnO_2 spheres have been synthesized using a one-step hydrothermal reaction with $SnCl_2{\cdot}2H_2O$ and KOH as raw materials. The morphology, microstructure, and optical properties of the products were characterized by X-ray powder diffraction (XRD), Raman spectrum, scanning electron microscopy (SEM), transmission electron microscopy (TEM), selected area electron diffraction (SAED), and ultraviolet-visible (UV-Vis) absorption spectroscopy. The detailed studies revealed that these synthesized spheres are highly monodisperse and have a uniform size of approximately 250 nm. Photocatalytic activity of the prepared SnO_2 spheres was evaluated by the degradation of methylene orange. The synthesized SnO_2 spheres exhibited excellent photocatalytic degradation. In addition, a possible formation mechanism of the walnut-like nanostructures was proposed based on reaction time-dependent experiments.

1. Introduction

Textile industries produce large volume of colored dye effluents which are toxic and nonbiodegradable [1]. In the past years, the traditional techniques for the treatment of dye waste effluents are usually inefficient, costly, and nondestructive or just transferring pollution from water to another phase [2]. Recently, the purification of wastewater by photocatalytic degradation of dyes using semiconductor particles has proven to be a very effective method, which leads to complete mineralization of the pollutants [3]. Many oxide semiconductors, such as TiO_2, ZnO, and SnO_2 [4–6], have been widely studied due to their good potential for photocatalyst. Among the above semiconductors, SnO_2 is a very important n-type oxide and wide band gap (3.6 eV) semiconductor [7]. Due to its excellent physicochemical properties, SnO_2 is employed in a wide range of applications, including gas sensors [8] and photocatalysts [9]. Some researchers have reported that heterogeneous SnO_2 showed enhanced photocatalytic activity for photodegradation of various organic dyes [10, 11]. However, use of SnO_2 single-phase as a photocatalyst to decompose organic dyes still remains difficult and necessary [12]. It is well known that the size and morphology of nanomaterials can substantially affect their physicochemical properties and their applications [13–15]. Therefore, novel SnO_2 morphologies may improve its performances in photocatalysis.

The hydrothermal method has been the most widely used method for synthesizing SnO_2 materials due to its advantages of saving energy and convenient manipulation as well as excellent control over size and morphology [16]. However, various templates and surfactants, which are typically toxic and expensive, are often introduced into the hydrothermal process to control the morphology, uniformity, and dispersibility of SnO_2 nanomaterials. The removal of these stabilizing molecules requires an additional thermal treatment or chemical etching. Alternatively, if SnO_2 nanomaterials could be synthesized via a hydrothermal reaction without any organic additive or template, the manipulation would be convenient and the extraneous impurities would be avoided. In this paper, we present a one-step hydrothermal method to prepare walnut-like SnO_2 spheres, using only $SnCl_2{\cdot}2H_2O$ and KOH as the raw materials. The products are investigated

in detail for their structural characteristics and morphologies. A possible growth mechanism of the walnut-like nanostructure is proposed based on the reaction time-dependent experiments. Furthermore, compared with the commercial SnO_2, the photocatalytic performance of the walnut-like SnO_2 is improved toward methyl orange (MO) solution.

2. Experimental Section

2.1. Material and Methods. All of the chemical reagents used in this research are of analytical grade without any further purification. In a typical synthesis, 0.002 mol of $SnCl_2{\cdot}2H_2O$ was dissolved in 35 mL of deionized water. Then, KOH (4 M, 5 mL) was added to the above solution under vigorous stirring at room temperature. The resulting solution was transferred to a Teflon-lined stainless steel autoclave (50 mL), sealed, and maintained at 190°C for 15 h. After cooling to room temperature, the obtained precipitates were washed several times with distilled water and absolute ethanol followed by drying at 60°C for 12 h.

2.2. Characterizations. X-ray powder diffraction (XRD) pattern was collected on a SmartLab X-ray diffractometer with Cu-Kα radiation (λ = 1.5406 Å). The Raman spectrum (inVia, Renishaw, Gloucestershire, UK) was excited by a 785 nm diode laser at room temperature. The morphologies of the samples were examined using Zeiss Supra 55 field emission scanning electron microscopy (FE-SEM) operated at 15 kV. Transmission electron microscopy (TEM, JEM-3010, Questar, New Hope, USA) was performed using an acceleration voltage of 300 kV. The optical absorption of the products was carried out using a UV-Vis double-beam spectrophotometer (UV-2450, SHIMADZU). The specific surface area was determined by the Brunauer-Emmett-Teller (BET) method using a surface area analyzer (Micromeritics, Gemini VII 2390).

2.3. Photodegradation Experiments. 0.05 g of the SnO_2 photocatalyst was dispersed in 50 mL of a 10 mg/L MO solution followed by stirring in the dark for 30 min to establish absorption equilibrium. Then, the suspension was irradiated by UV light (300 W mercury lamp) under continuous magnetic stirring. After irradiation for a certain time period, the reaction suspension was centrifuged and characterized using a UV-Vis spectrophotometer.

3. Results and Discussion

The XRD pattern of the walnut-like SnO_2 spheres is shown in Figure 1. All of the diffraction peaks are able to index to the tetragonal rutile structure of SnO_2 based on both the position and relative intensity (JCPDS Card number 71-0652). There is no other peak detected, which indicates that the as-prepared SnO_2 product has high purity. The sharp diffraction peaks imply that the walnut-like SnO_2 sphere in this work is highly crystalline. Based on the Debby-Scherer equation ($d = k\lambda/B\cos\theta$, where d is the mean crystalline size of the powder, λ is the wavelength of Cu-Kα (λ = 1.5406 Å), B is the full width at half maximum (FWHM) intensity of the peak

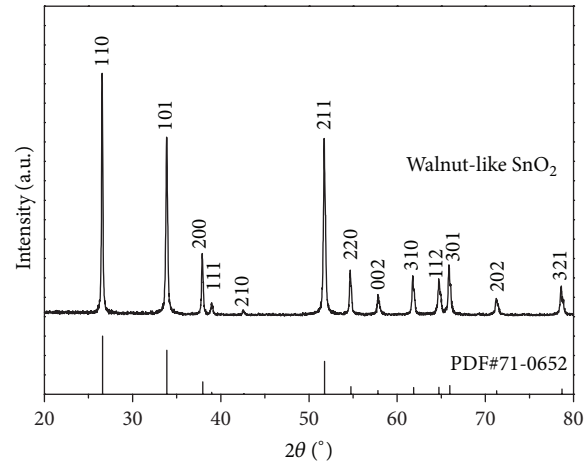

Figure 1: XRD pattern of the as-prepared walnut-like SnO_2 spheres.

in radian, θ is Bragg's diffraction angle, and k is a constant usually equal to ~0.9) [17], the average crystallite size of SnO_2 calculated from the main diffraction peak is about 43 nm.

The images in Figures 2(a)–2(d) show the morphologies of the products prepared with different concentration of KOH. It is found that the concentration of KOH affects the morphology dramatically. When the KOH concentration was 2 M, the product consists of dispersed nanoplates (Figure 2(a)). The size of some nanoplates is about 400 nm. As the concentration increases to 3 M, some hierarchical structures begin to appear (Figure 2(b)). It can be seen from some broken hierarchical structures that the inner of the products consists of tiny nanoparticles and the surface of the products is covered with numerous nanoplates. Additionally, compared with the concentration of 2 M, the size of nanoplates of the hierarchical structures decreases to ~200 nm. With an increase of concentration to 4 M, walnut-like SnO_2 spheres are obtained (Figure 2(c)). These SnO_2 spheres are highly monodisperse and have a uniform diameter of approximately 250 nm. From the high magnification SEM image (Figure 2(d)), it can be seen that the surface of walnut-like SnO_2 spheres has many edges, which interlaced with each other to form uniform walnut-like appearance. It denotes that the preferential adsorption of molecules and ions from solution on different crystal faces directs the anisotropic growth of nanoparticles by controlling the growth rate along different crystal axes [18]. Yang et al. proposed that OH^- ions attached favorably to the specific facets of rutile SnO_2 nanocrystals and accelerated the growth rate of these facets [19]. Our results indicate that the KOH influence the anisotropic growth of SnO_2 and play an important role in the synthesis of walnut-like structure.

To investigate the growth process of the walnut-like SnO_2 spheres and the possible growth mechanism, reaction time-dependent experiments were performed. The corresponding results are shown in Figures 3(a)–3(d). When the hydrothermal time is 4 h, the product consists of some aggregates with sharp corners (Figure 3(a)). When the hydrothermal reaction time is prolonged to 6 h, the nanostructure evolves

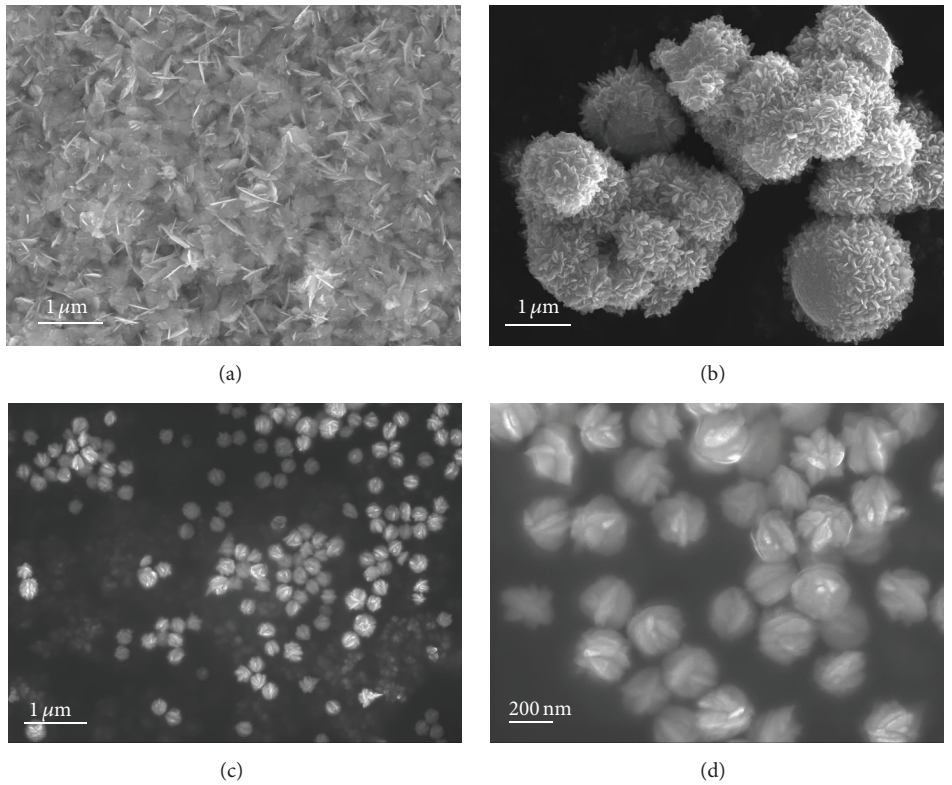

(a) (b) (c) (d)

Figure 2: SEM images of the samples obtained with various KOH concentrations for 15 h: (a) 2 M, (b) 3 M, (c) 4 M, and (d) 4 M at high magnification.

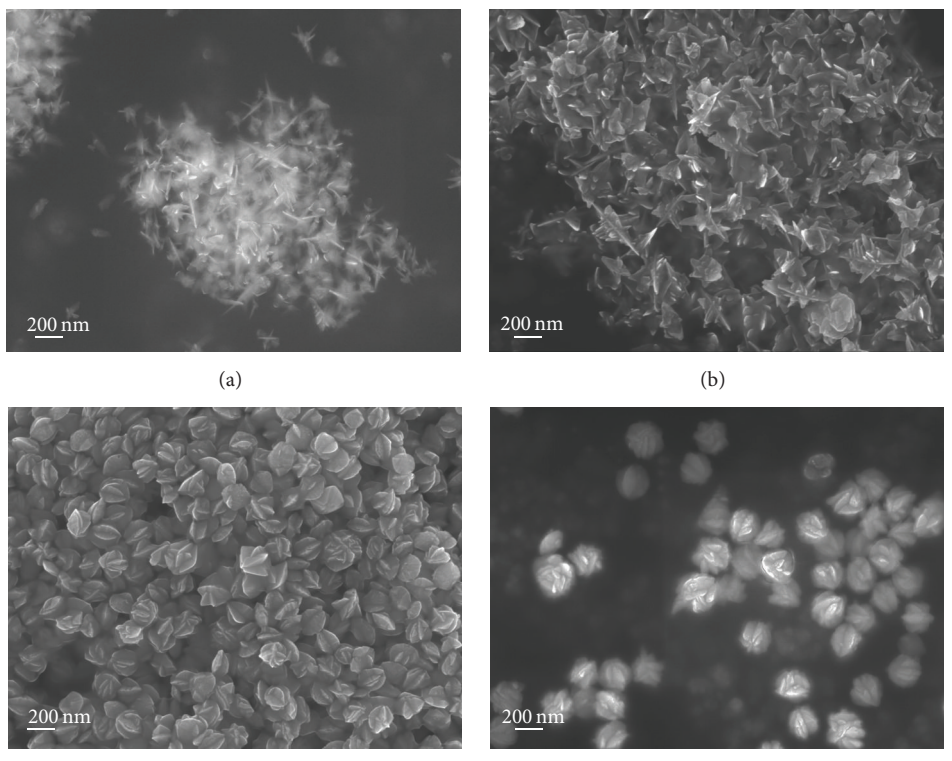

(a) (b) (c) (d)

Figure 3: SEM images of the SnO_2 products prepared with 4 M KOH for (a) 4 h, (b) 6 h, (c) 12 h, and (d) 15 h.

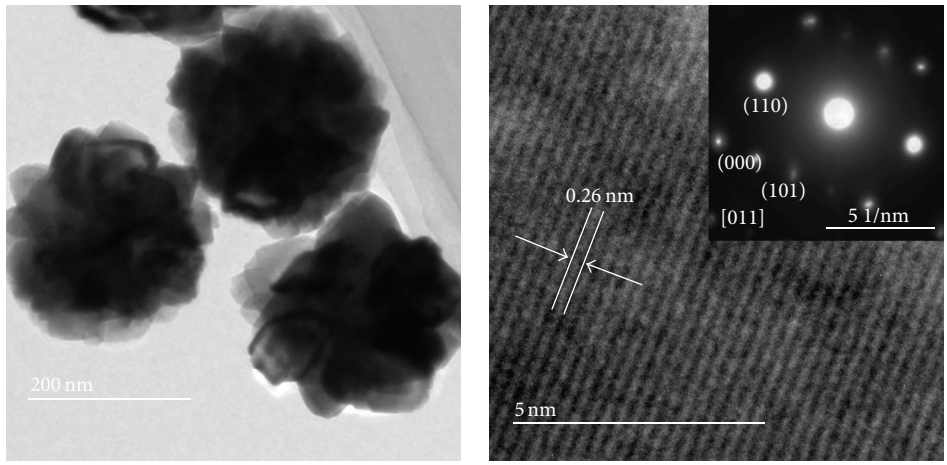

(a) (b)

Figure 4: (a) TEM and (b) HRTEM and SAED pattern (inset) images of walnut-like SnO_2 spheres.

into the irregular aggregates assembled by imperfect plates (Figure 3(b)). Additionally, the surface of these plates is rough, where some tiny nanoparticles are enchased. When the reaction time is further prolonged to 12 h, the structure evolves into spheres and ellipsoids with wrinkly surface (Figure 3(c)). Compared with the product obtained at 6 h, the edges of these spheres or ellipsoids become obviously smoother and thicker. After increasing the reaction time to 15 h, walnut-like spheres are obtained (Figure 3(d)).

To obtain more details of the walnut-like SnO_2 spheres, the structure is characterized by TEM and SAED. As shown in Figure 4(a), the products have a spherical appearance with an average size of ~250 nm, which agrees with the results from SEM. Furthermore, the as-prepared SnO_2 spheres are solid and composed of some nanoparticles. Figure 4(b) shows high-resolution TEM (HRTEM) image and selected area electron diffraction (SAED) pattern (inset of Figure 4(b)), respectively. Based on the HRTEM image, the measured d-spacing is 0.26 nm, which corresponds to the (101) planes of the tetragonal rutile SnO_2. The sharp diffraction spots observed in the SAED pattern indicate that the individual nanoparticles are highly crystalline. Furthermore, the spots can be easily divided into two sets, which are caused by the (101) and (110) crystal planes, and correspond to the [011] zone axis. These crystallographic results agree well with the XRD analysis.

Based on the experimental results, a formation mechanism is proposed, as illustrated in Figure 5. The reaction at basic conditions can be shown as follows [19–22]:

$$Sn^{2+} + 2H_2O \longrightarrow Sn(OH)_2 + 2H^+ \quad (1)$$

$$Sn(OH)_2 \longrightarrow SnO + H_2O \quad (2)$$

$$SnO + \frac{1}{2}O_2 \longrightarrow SnO_2 \quad (3)$$

$$Sn(OH)_2 + \frac{1}{2}O_2 + H_2O \longrightarrow Sn(OH)_4 \quad (4)$$

$$Sn(OH)_4 + 2OH^- \longrightarrow Sn(OH)_6^{2-} \quad (5)$$

$$Sn(OH)_6^{2-} \longrightarrow SnO_2 + 2OH^- + 2H_2O \quad (6)$$

When $SnCl_2{\cdot}2H_2O$ is added into the water, the $Sn(OH)_2$ is obtained efficiently by the rapid hydrolysis of Sn^{2+} cations (see (1)), and some of them further undergo dehydration and oxidation to form SnO_2 (see (2)-(3)), while some others are subsequently oxidized to produce $Sn(OH)_4$ precipitation (see (4)). When KOH is added into the solution, the amphoteric $Sn(OH)_4$ precipitations immediately react with the excessive OH^- to produce dissoluble $Sn(OH)_6^{2-}$ complex ions (see (5)). During hydrothermal treatment, the complex $Sn(OH)_6^{2-}$ ions decompose and massive SnO_2 nuclei are formed (see (6)) [23]. In the present study, the formation of walnut-like structure is a typical Ostwald ripening process. At first, the supersaturation of reaction system is high; thus the nucleation is dominant. Large quantities of SnO_2 nuclei or particles aggregate to reduce the overall Gibbs free energy [24]. Subsequently, SnO_2 nuclei or particles grow preferentially with growth inhibition in the [001] direction to form platy structure [19]. In the latter stage, the nucleation is gradually reduced as the supersaturation falls with time in the surrounding solution. The new nucleated particles spontaneously "land" on the as-formed larger plates because of the surface energy minimization and further grow into another plate, leading to the irregular assembly [25]. When the reaction is further progressed, the nucleation stops because the concentration falls below the critical nucleation concentration [26]. However, the dissolution and recrystallization process through the competition growth under Ostwald ripening process still continue [27, 28]. Therefore, the larger SnO_2 plates grow at the cost of the smaller ones due to the different solubility between relatively larger and smaller particles. Then the thickness of these larger SnO_2 plates increases gradually. Also, their edge becomes smoother. Finally, walnut-like SnO_2 spheres are formed as the reaction time is further extended to 15 h.

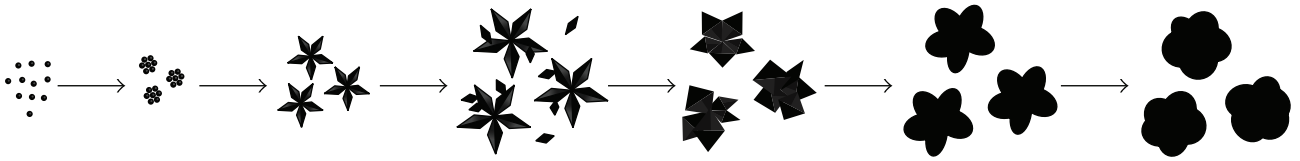

Figure 5: Schematic formation mechanism of walnut-like SnO_2 spheres.

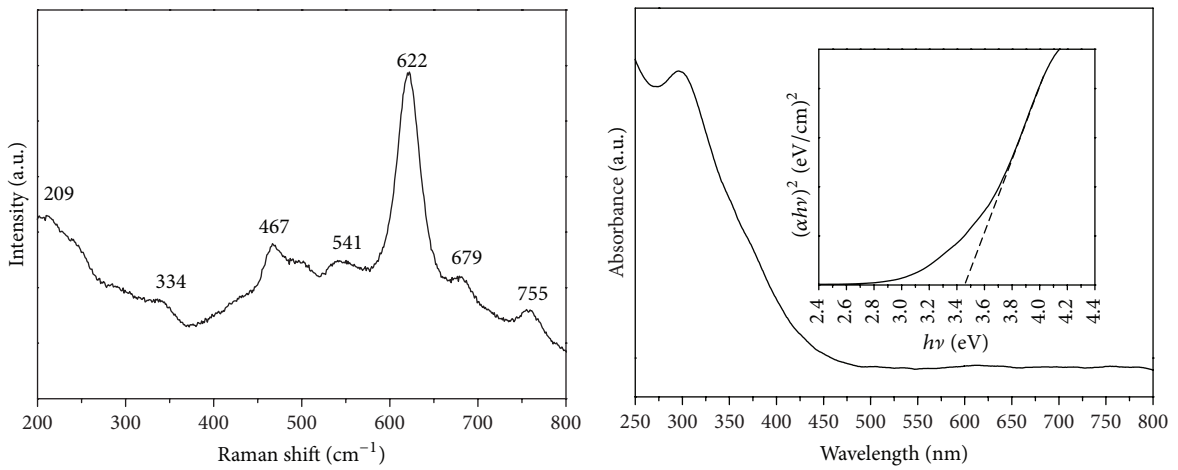

Figure 6: (a) Raman spectrum and (b) UV-Vis absorption spectrum and plots of $(\alpha h\nu)^2$ versus $h\nu$ (inset) of walnut-like SnO_2 spheres.

As is well known, Raman spectroscopy is a powerful method for the investigation of the structural properties of nanoparticles, because the variations in Raman spectra with decreases in particle size can be easily detected [29]. The tetragonal rutile SnO_2 belongs to the space group D_{4h}, of which the normal lattice vibration at the Γ point of the Brillouin Zone is given by the following equation [30, 31]:

$$\Gamma = 1A_{1g} + 1A_{2g} + 1A_{2u} + 1B_{1g} + 1B_{2g} + 2B_{1u} + 1E_g + 3E_u. \quad (7)$$

Among these modes, A_{1g}, E_g, B_{1g}, and B_{2g} modes are Raman active; A_{2u} and $3E_u$ modes are IR active; and $2B_{1u}$ and A_{2g} modes are inactive. Figure 6(a) shows the Raman spectrum of the walnut-like SnO_2 spheres at room temperature. The Raman peaks located at 467, 622, and 755 cm^{-1} were assigned to the E_g, A_{1g}, and B_{2g} vibrational modes of tetragonal rutile SnO_2, respectively. These peaks show that the walnut-like SnO_2 spheres actually possess the main optical characteristics of a tetragonal rutile structure. In addition to these classical vibration modes, some additional Raman scattering peaks at 209, 334, 541, and 679 cm^{-1}, which are not found in Raman spectrum of bulk SnO_2 crystals, can be observed in the present SnO_2 spheres. According to some previous studies [32–34], the peak at 334 cm^{-1} may be related to the surface defects or the SnO_2 nanocluster formation, which constituted a new kind of vibration mode. The 209 cm^{-1} peak position is similar to the Eu(TO) mode observed in the IR spectra of crystalline SnO_2 [35, 36]. The 679 cm^{-1} peaks and the 541 cm^{-1} peak correspond to the A_{2u} mode [37, 38] and inactive B_{1u} mode [39], respectively. These additional Raman peaks can be explained as follows. As particle size decreases due to the increase in the surface-to-volume ratio, the surface modes become dominant and some new bands may be observed. In the present SnO_2 spheres, the presence of IR modes and other forbidden Raman modes can be attributed to the relaxation of the Raman selection rules purportedly due to the reduced dimension of the nanostructure, as well as the lattice disorder and a high concentration of defects such as oxygen vacancies [40]. Another feature observed on Raman spectrum is that the peaks shifts can be found by comparing with the data from bulk SnO_2 [41]. This is consistent with the findings reported by others, which can be explained using phonon dispersion [42–44].

The UV-Vis absorption spectrum of the walnut-like SnO_2 spheres is shown in Figure 6(b). The band gap can be determined by $(\alpha h\nu)^2 = A(h\nu - E_g)$, where α, A, and $h\nu$ are the absorption coefficient, a constant, and the photon energy, respectively [45]. According to the intercept of the tangent to the plot of $(\alpha h\nu)^2$ as a function of ν, the band gap is approximately equal to 3.46 eV (inset of Figure 6(b)), which is lower than that for bulk SnO_2.

The experiments related to photocatalytic degradation of MO were carried out to demonstrate the photocatalytic properties of walnut-like SnO_2 nanospheres. Figure 7(a) shows the photocatalytic rate of walnut-like SnO_2 spheres and commercial SnO_2 powders under UV light at different periods of time. After 180 min of illumination, in the case of

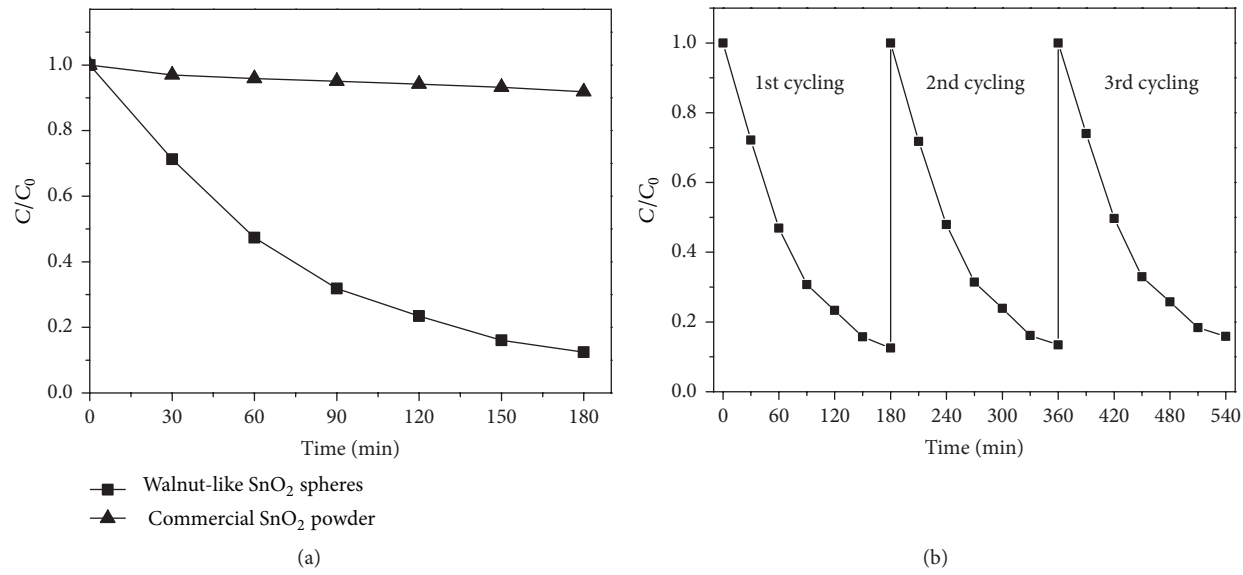

FIGURE 7: (a) Photocatalytic degradation of MO under UV irradiation and (b) stability for photocatalytic activity of walnut-like SnO_2 spheres.

walnut-like SnO_2 spheres, the degradation of the MO concentration is about 88%, whereas in the case of commercial one, the degradation is lower than 9%. In order to evaluate the photostability, the cyclic photodegradation of MO over the walnut-like SnO_2 spheres is also examined. As shown in Figure 7(b), after three cycles of photocatalytic degradation, no significant loss of activity is represented. It indicates that the photocatalysts with high photocatalytic activity could be easily recovered by sedimentation and would greatly promote their industrial application in eliminating organic pollutants from wastewater.

The basic photocatalytic principle relies on the photogenerated electrons (e^-) and holes (h^+) (when absorbed energy is equal to or higher than its band gap) [1]. The electrons and holes react with the adsorbed surface substances, like O_2 and OH^-, to form reactive species $^{\bullet}O^{2-}$ and $OH^{\bullet}$, which are the major oxidative species for the decomposition of organic pollutants. Generally, the larger exposed surface can provide more surface sites, where $OH^{\bullet}$ radicals can be generated by the reaction between the photogenerated charge carriers and react with MO molecule. The as-prepared SnO_2 spheres possess the small size and rough surface, which benefit from improving their specific surface area. The BET surface area of the walnut-like SnO_2 spheres is estimated by nitrogen sorption and is about 47.4 m^2g^{-1}, which is much higher than that of the commercial SnO_2 (3.5 m^2g^{-1}). Moreover, the walnut-like SnO_2 spheres are highly monodisperse without agglomeration in the solution. This good dispersion stability is of considerable importance in the practical water treatment applications.

4. Conclusions

Novel walnut-like SnO_2 spheres have been synthesized successfully via a facile one-step hydrothermal method. The as-prepared SnO_2 spheres are highly monodisperse and have a uniform size of approximately 250 nm. The formation mechanism of the SnO_2 walnut-like structure has been proposed. In addition, these walnut-like SnO_2 spheres exhibit excellent photoactivity for the degradation of MO. Our synthesis method is environmental-friendly and inexpensive. It provides SnO_2 materials with a novel morphology that can be exploited for various applications.

Conflict of Interests

The authors declare that there is no conflict of interests regarding the publication of this paper.

Acknowledgments

This work was supported by the National Natural Science Foundation of China (51172187, 51277138, 51402230, and 61405151), SPDRF (20116102130002), 111 Program of MOE (B08040), the Natural Science Foundation of Shaanxi Province (nos. 2014JQ8337 and 2013KW12-02), the Scientific Research Program of Shaanxi Education Department (nos. 15JK1325 and 15JK1578), the Doctorate Foundation (BS1436) of China, the SKLP Foundation (KP201421), and the Fundamental Research Funds for the Central Universities (3102014JGY01004) of China.

References

[1] S. K. Kansal, M. Singh, and D. Sud, "Studies on photodegradation of two commercial dyes in aqueous phase using different photocatalysts," *Journal of Hazardous Materials*, vol. 141, no. 3, pp. 581–590, 2007.

[2] J. Xie, H. Wang, M. Duan, and L. Zhang, "Synthesis and photocatalysis properties of ZnO structures with different morphologies via hydrothermal method," *Applied Surface Science*, vol. 257, no. 15, pp. 6358–6363, 2011.

[3] H. Zhang and C. Hu, "Effective solar absorption and radial microchannels of SnO_2 hierarchical structure for high photocatalytic activity," *Catalysis Communications*, vol. 14, no. 1, pp. 32–36, 2011.

[4] E. Kusvuran, A. Samil, O. M. Atanur, and O. Erbatur, "Photocatalytic degradation kinetics of di- and tri-substituted phenolic compounds in aqueous solution by TiO_2/UV," *Applied Catalysis B: Environmental*, vol. 58, no. 3-4, pp. 211–216, 2005.

[5] S. A. Khayyat, M. S. Akhtar, and A. Umar, "ZnO nanocapsules for photocatalytic degradation of thionine," *Materials Letters*, vol. 81, no. 4, pp. 239–241, 2012.

[6] S. Jana, B. C. Mitra, P. Bera, M. Sikdar, and A. Mondal, "Photocatalytic activity of galvanically synthesized nanostructure SnO_2 thin films," *Journal of Alloys and Compounds*, vol. 602, no. 2, pp. 42–48, 2014.

[7] Z. Chen, D. Pan, Z. Li et al., "Recent advances in tin dioxide materials: some developments in thin films, nanowires, and nanorods," *Chemical Reviews*, vol. 114, no. 15, pp. 7442–7486, 2014.

[8] Y. Li, L. Qiao, L. Wang, Y. Zeng, W. Fu, and H. Yang, "Synthesis of self-assembled 3D hollow microspheres of SnO_2 with an enhanced gas sensing performance," *Applied Surface Science*, vol. 285, no. 19, pp. 130–135, 2013.

[9] W.-W. Wang, Y.-J. Zhu, and L.-X. Yang, "ZnO-SnO_2 hollow spheres and hierarchical nanosheets: hydrothermal preparation, formation mechanism, and photocatalytic properties," *Advanced Functional Materials*, vol. 17, no. 1, pp. 59–64, 2007.

[10] J. Yuan, X. Zhang, H. Li et al., "TiO_2/SnO_2 double-shelled hollow spheres-highly efficient photocatalyst for the degradation of rhodamine B," *Catalysis Communications*, vol. 60, pp. 129–133, 2015.

[11] W. Zhou, Y. Y. Tay, X. Jia et al., "Controlled growth of SnO_2@Fe_2O_3 double-sided nanocombs as anodes for lithium-ion batteries," *Nanoscale*, vol. 4, no. 15, pp. 4459–4463, 2012.

[12] H. Chen, D. Zhang, X. Zhou, J. Zhu, X. Chen, and X. Zeng, "Controllable construction of ordered porous SnO_2 nanostructures and their application in photocatalysis," *Materials Letters*, vol. 116, no. 2, pp. 127–130, 2014.

[13] A. Kar, S. Kundu, and A. Patra, "Surface defect-related luminescence properties of SnO_2 nanorods and nanoparticles," *Journal of Physical Chemistry C*, vol. 115, no. 1, pp. 118–124, 2011.

[14] H. Wang and A. L. Rogach, "Hierarchical SnO_2 nanostructures: recent advances in design, synthesis, and applications," *Chemistry of Materials*, vol. 26, no. 1, pp. 123–133, 2014.

[15] Q. Zhao, D. Ju, X. Deng, J. Huang, B. Cao, and X. Xu, "Morphology-modulation of SnO_2 hierarchical architectures by Zn doping for glycol gas sensing and photocatalytic applications," *Scientific Reports*, vol. 5, no. 7874, pp. 1–9, 2015.

[16] W. Shi, S. Song, and H. Zhang, "Hydrothermal synthetic strategies of inorganic semiconducting nanostructures," *Chemical Society Reviews*, vol. 42, no. 13, pp. 5714–5743, 2013.

[17] A. L. Patterson, "The scherrer formula for X-ray particle size determination," *Physical Review*, vol. 56, no. 10, pp. 978–982, 1939.

[18] C. J. Murphy, "Materials science: Nanocubes and nanoboxes," *Science*, vol. 298, no. 5601, pp. 2139–2141, 2002.

[19] R. Yang, Y. Gu, Y. Li, J. Zheng, and X. Li, "Self-assembled 3-D flower-shaped SnO_2 nanostructures with improved electrochemical performance for lithium storage," *Acta Materialia*, vol. 58, no. 3, pp. 866–874, 2010.

[20] B. Mehrabi Matin, Y. Mortazavi, A. A. Khodadadi, A. Abbasi, and A. Anaraki Firooz, "Alkaline- and template-free hydrothermal synthesis of stable SnO_2 nanoparticles and nanorods for CO and ethanol gas sensing," *Sensors and Actuators, B: Chemical*, vol. 151, no. 1, pp. 140–145, 2010.

[21] H. Z. Wang, J. B. Liang, H. Fan et al., "Synthesis and gas sensitivities of SnO_2 nanorods and hollow microspheres," *Journal of Solid State Chemistry*, vol. 181, no. 1, pp. 122–129, 2008.

[22] H. Zhang, W. Zeng, J. Hao, Y. Li, and B. Miao, "Hydrothermal synthesis of flower-like SnO_2 architectures with superior gas sensing properties," *Materials Letters*, vol. 145, no. 15, pp. 133–136, 2015.

[23] L. Wang, S. Wang, Y. Wang, H. Zhang, Y. Kang, and W. Huang, "Synthesis of hierarchical SnO_2 nanostructures assembled with nanosheets and their improved gas sensing properties," *Sensors and Actuators B: Chemical*, vol. 188, pp. 85–93, 2013.

[24] S. Liu, G. Huang, J. Yu, T. W. Ng, H. Y. Yip, and P. K. Wong, "Porous fluorinated SnO_2 hollow nanospheres: transformative self-assembly and photocatalytic inactivation of bacteria," *ACS Applied Materials and Interfaces*, vol. 6, no. 4, pp. 2407–2414, 2014.

[25] Y. Liu, Y. Jiao, Z. Zhang, F. Qu, A. Umar, and X. Wu, "Hierarchical SnO_2 nanostructures made of intermingled ultrathin nanosheets for environmental remediation, smart gas sensor, and supercapacitor applications," *ACS Applied Materials and Interfaces*, vol. 6, no. 3, pp. 2174–2184, 2014.

[26] Y. Wang, J. Tian, C. Fei et al., "Microwave-assisted synthesis of SnO_2 nanosheets photoanodes for dye-sensitized solar cells," *The Journal of Physical Chemistry C*, vol. 118, no. 45, pp. 25931–25938, 2014.

[27] X. W. Lou, L. A. Archer, and Z. C. Yang, "Hollow micro-/nanostructures: synthesis and applications," *Advanced Materials*, vol. 20, no. 21, pp. 3987–4019, 2008.

[28] P. Sun, W. Zhao, Y. Cao, Y. Guan, Y. Sun, and G. Lu, "Porous SnO_2 hierarchical nanosheets: hydrothermal preparation, growth mechanism, and gas sensing properties," *CrystEngComm*, vol. 13, no. 11, pp. 3718–3724, 2011.

[29] H. C. Choi, Y. M. Jung, and S. B. Kim, "Size effects in the Raman spectra of TiO_2 nanoparticles," *Vibrational Spectroscopy*, vol. 37, no. 1, pp. 33–38, 2005.

[30] J. Kaur, J. Shah, R. K. Kotnala, and K. C. Verma, "Raman spectra, photoluminescence and ferromagnetism of pure, Co and Fe doped SnO_2 nanoparticles," *Ceramics International*, vol. 38, no. 7, pp. 5563–5570, 2012.

[31] K. Srinivas, M. Vithal, B. Sreedhar, M. M. Raja, and P. V. Reddy, "Structural, optical, and magnetic properties of nanocrystalline Co doped SnO_2 based diluted magnetic semiconductors," *The Journal of Physical Chemistry C*, vol. 113, no. 9, pp. 3543–3552, 2009.

[32] M. Ristić, M. Ivanda, S. Popović, and S. Musić, "Dependence of nanocrystalline SnO_2 particle size on synthesis route," *Journal of Non-Crystalline Solids*, vol. 303, no. 2, pp. 270–280, 2002.

[33] M. N. Rumyantseva, A. M. Gaskov, N. Rosman, T. Pagnier, and J. R. Morante, "Raman surface vibration modes in nanocrystalline SnO_2: correlation with gas sensor performances," *Chemistry of Materials*, vol. 17, no. 4, pp. 893–901, 2005.

[34] K. N. Yu, Y. Xiong, Y. Liu, and C. Xiong, "Microstructural change of nano-SnO_2 grain assemblages with the annealing temperature," *Physical Review B*, vol. 55, no. 4, pp. 2666–2671, 1997.

[35] Y. Liu, Y. Dong, and G. Wang, "Far-infrared absorption spectra and properties of SnO_2 nanorods," *Applied Physics Letters*, vol. 82, no. 2, pp. 260–262, 2003.

[36] Y. Liu, C. Zheng, W. Wang, C. Yin, and G. Wang, "Synthesis and characterization of rutile SnO_2 nanorods," *Advanced Materials*, vol. 13, no. 24, pp. 1883–1887, 2001.

[37] S. Loridant, "Determination of the maximum vanadium oxide coverage on SnO_2 with a high surface area by Raman spectroscopy," *Journal of Physical Chemistry B*, vol. 106, no. 51, pp. 13273–13279, 2002.

[38] C. G. Granqvist and A. Hultåker, "Transparent and conducting ITO films: new developments and applications," *Thin Solid Films*, vol. 411, no. 1, pp. 1–5, 2002.

[39] M. Batzill and U. Diebold, "The surface and materials science of tin oxide," *Progress in Surface Science*, vol. 79, no. 2–4, pp. 47–154, 2005.

[40] T. Livneh, Y. Lilach, I. Popov, A. Kolmakov, and M. Moskovits, "Polarized raman scattering from a single, segmented SnO_2 wire," *Journal of Physical Chemistry C*, vol. 115, no. 35, pp. 17270–17277, 2011.

[41] R. S. Katiyar, P. Dawson, M. M. Hargreave, and G. R. Wilkinson, "Dynamics of the rutile structure. III. Lattice dynamics, infrared and Raman spectra of SnO_2," *Journal of Physics C: Solid State Physics*, vol. 4, no. 15, pp. 2421–2431, 1971.

[42] A. Diéguez, A. Romano-Rodríguez, A. Vilà, and J. R. Morante, "The complete Raman spectrum of nanometric SnO_2 particles," *Journal of Applied Physics*, vol. 90, no. 3, pp. 1550–1557, 2001.

[43] G. Xi and J. Ye, "Ultrathin SnO_2 nanorods: template- and surfactant-free solution phase synthesis, growth mechanism, optical, gas-sensing, and surface adsorption properties," *Inorganic Chemistry*, vol. 49, no. 5, pp. 2302–2309, 2010.

[44] S. Mehraj, M. S. Ansari, and Alimuddin, "Structural, electrical and magnetic properties of (Fe, Co) co-doped SnO_2 diluted magnetic semiconductor nanostructures," *Physica E*, vol. 65, pp. 84–92, 2015.

[45] G.-W. Chu, Q.-H. Zeng, Z.-G. Shen, H.-K. Zou, and J.-F. Chen, "Preparation of SnO_2 nanoparticles using a helical tube reactor via continuous hydrothermal route," *Chemical Engineering Journal*, vol. 253, no. 7, pp. 78–83, 2014.